ISSN No:-2456-2165 https://doi.org/10.38124/ijisrt/26aug788

Integrated Multisource Geophysical and Remote Sensing Data Fusion for Mineral Prospectivity Mapping: A Reproducible Framework Applied to the Olympic Cu–Au Province, Gawler Craton, South Australia

Okeke Sunday Okechukwu[1*]; Okonkwo Churchill Chukwunonso[2]; Achilike Kennedy Okechukwu[3]

[1;2]Department of Physics Education, School of Science, Federal College of Education (Technical), Umunze, Anambra State, Nigeria
[3]Department of Physics, Faculty of Biological and Physical Sciences, Abia State University, Uturu, Abia State, Nigeria

Corresponding Author: Okeke Sunday Okechukwu[1*]

Publication Date: 2026/08/31

Abstract: Mineral exploration in covered and structurally complex terranes increasingly relies on the integration of complementary evidence layers rather than any single dataset. This study presents a reproducible, open-data workflow for mineral prospectivity mapping (MPM) that fuses multispectral and thermal remote sensing, potential-field and radiometric geophysics, and public geological and mineral-occurrence data within a common geographic information system (GIS) framework. The workflow combines knowledge-driven fuzzy logic, data-driven weights-of-evidence, and a machine-learning ensemble (random forest with gradient-boosted refinement) through a stacked meta-learner, and is validated using spatial k-fold cross-validation, receiver operating characteristic (ROC) analysis, and prediction-rate curves referenced against independent occurrence subsets. We demonstrate the framework on the Olympic Cu–Au Province of the Gawler Craton, South Australia — a world-class, largely covered iron oxide copper-gold (IOCG) system for which regional gravity, aeromagnetic, radiometric, magnetotelluric, and geological data are openly available through national and state geoscience portals. Evidence layers derived from reduced-to-pole magnetics, residual Bouguer gravity, radioelement ratios, ASTER-derived alteration indices, structural lineament density, and lithological favorability are standardized to a common 30 m grid and integrated using the proposed fusion architecture. Consistent with published mineral-systems studies of the province, structural and magnetic-gravity evidence layers emerge as the strongest predictors of IOCG favorability, with alteration and radiometric layers providing secondary but non-redundant discrimination. We discuss the comparative advantages of ensemble fusion over single-source and single-method approaches, the sensitivity of prospectivity outputs to training-occurrence bias, and the practical steps required to operationalize the framework using entirely open datasets. The methodology, code structure, and evidence-layer catalogue are provided to support reproducibility and transfer to other covered metallogenic provinces.

Keywords: *Mineral Prospectivity Mapping; Data Fusion; Remote Sensing; Potential-Field Geophysics; Machine Learning; Weights of Evidence; Fuzzy Logic; IOCG Deposits; Gawler Craton; Open Geoscience Data.*

How to Cite: Okeke Sunday Okechukwu; Okonkwo Churchill Chukwunonso; Achilike Kennedy Okechukwu (2026) Integrated Multisource Geophysical and Remote Sensing Data Fusion for Mineral Prospectivity Mapping: A Reproducible Framework Applied to the Olympic Cu–Au Province, Gawler Craton, South Australia. *International Journal of Innovative Science and Research Technology*, 11(8), 2148-2157. https://doi.org/10.38124/ijisrt/26aug788

I. INTRODUCTION

Global demand for copper, gold, and critical minerals has renewed interest in exploration strategies capable of detecting deposits beneath post-mineral cover, where outcrop-based prospecting is no longer sufficient (Müller et al., 2025). Mineral prospectivity mapping (MPM) the spatial prediction of the relative likelihood of mineral occurrence

ISSN No:-2456-2165 https://doi.org/10.38124/ijisrt/26aug788

from geoscientific evidence has become a standard tool for prioritizing greenfield and brownfield exploration targets under these conditions (Yousefi et al., 2021; Carranza, 2008). Historically, MPM relied on single data types, most commonly geochemical or geological maps, interpreted through expert judgment (Bonham-Carter, 1994; Porwal & Kreuzer, 2010). Over the past two decades, however, the field has shifted toward integrating multiple, independent evidence sources (Yousefi et al., 2021; Shirmard et al., 2022): multispectral and hyperspectral remote sensing for surface alteration and lithological discrimination (Pour & Hashim, 2012; Hajaj et al., 2024a); airborne and ground potential-field geophysics for subsurface structure and rock-property contrasts (Abubakar & Abir, 2025); radiometric surveys for near-surface geochemical proxies (Olomo et al., 2022); and geological, structural, and mineral-occurrence databases for genetic context (Carranza, 2008).

The rationale for multisource fusion is straightforward: individual data types are each sensitive to only part of the mineral system (Porwal & Kreuzer, 2010). Remote sensing captures near-surface alteration mineralogy but is blind beneath even shallow cover or vegetation (Pour & Hashim, 2012); potential-field geophysics resolves subsurface density and susceptibility contrasts but cannot directly discriminate mineralogy; and geochemical or radiometric data are typically restricted to near-surface expression. Deposits form through the coincidence of multiple favorable conditions a fertile source, an efficient transport pathway, and a depositional trap and no single dataset images all three (Thapa & Pokhrel, 2025). A substantial body of work has therefore explored how to combine heterogeneous evidence layers into a single, defensible prospectivity output, using knowledge-driven methods such as fuzzy logic and Boolean overlay, data-driven statistical methods such as weights-of-evidence (WofE) and logistic regression, and, increasingly, machine-learning (ML) and deep-learning methods including random forest, support vector machines, and convolutional neural networks.

Recent studies consistently note two trends (Shirmard et al., 2022; Hajaj et al., 2024a). First, machine-learning approaches applied to remote sensing and multi-source geoscience data have proliferated rapidly, with random forest and its ensemble variants remaining the most widely adopted classifiers because of their robustness to noisy, correlated, and mixed-type evidence layers, and their capacity to report variable importance for geological interpretation (Sun et al., 2019; Xiong et al., 2018). Second, the transition from single-source to genuinely multi-source fusion has been identified as the key driver of improved predictive performance, with hybrid and ensemble methods reported to increase prediction accuracy over single-method baselines in complex mineral systems (Yang et al., 2022). At the same time, most published case studies remain method-specific comparing, for example, WofE against fuzzy logic, or one ML classifier against another rather than presenting an end-to-end, fully reproducible fusion architecture that combines knowledge-driven, data-driven, and machine-learning components within a single validated pipeline, built entirely from openly licensed data.

This gap matters for two reasons. First, exploration organizations, especially those in the junior and academic sectors, increasingly require workflows that can be executed without proprietary survey data, since open government geoscience portals (e.g., national geological surveys, Copernicus, and USGS/NASA missions) now provide sufficient coverage for regional-scale MPM in many jurisdictions. Second, journal referees and downstream users of prospectivity maps increasingly expect transparent validation cross-validated ROC/AUC and prediction-rate curves referenced against independent occurrence subsets rather than qualitative overlay maps whose predictive skill cannot be independently checked.

II. METHODOLOGY

- *Study Area: The Olympic Cu–Au Province, Gawler Craton*

The Gawler Craton of South Australia is an Archean to Mesoproterozoic crustal block that hosts one of the world's most richly endowed iron oxide copper-gold (IOCG) provinces, the Olympic Cu–Au Province, in its eastern portion. This province contains the supergiant Olympic Dam Cu–U–Au–Ag deposit together with the major Prominent Hill, Carrapateena, and Wirrda Well IOCG deposits, and hosts numerous additional prospects along a north–south metallogenic corridor associated with a fundamental lithospheric boundary active during Mesoproterozoic (c. 1.6 Ga) magmatism and hydrothermal alteration.

The province is an especially instructive test case for multisource data fusion because it is almost entirely concealed beneath post-mineral Neoproterozoic–Cambrian sedimentary cover, meaning that direct geological mapping of the mineralized basement is not possible over most of the area and exploration success depends heavily on geophysical and indirect surface-expression evidence. This has made the Gawler Craton the subject of sustained public investment in regional geophysics — including gravity, aeromagnetics, radiometrics, deep crustal seismic reflection profiles, and, more recently, three-dimensional magnetotelluric (AusLAMP) surveys — much of which is released as open data through Geoscience Australia and the South Australian Resources Information Gateway (SARIG). Published mineral-systems studies of the province have already used weights-of-evidence and knowledge-driven prospectivity models to rank the Olympic Cu-Au Province and the adjacent Curnamona Province for further IOCG discovery (Skirrow et al., 2019; Katona et al., 2018), providing a robust literature baseline against which a new fusion framework's outputs can be qualitatively benchmarked.

IOCG mineralisation in the province is associated with both hematite- and magnetite-rich alteration assemblages, with hematite-rich systems considered the most economically significant (Reid, 2019). Regional controls recognized in the mineral-systems literature include: (i) crustal-to lithospheric-scale structures and their intersections, imaged through gravity and magnetic gradient/lineament analysis; (ii) coincident gravity and magnetic anomalies reflecting iron-oxide-rich alteration haloes; (iii) elevated potassium and

ISSN No:-2456-2165 https://doi.org/10.38124/ijisrt/26aug788

depleted thorium/uranium radiometric signatures associated with potassic alteration, where exposed; and (iv) anomalous lithospheric mantle electrical conductivity imaged by magnetotelluric surveys, interpreted to reflect metasomatized, fertile mantle beneath the province. These multiple, only partially overlapping geophysical footprints make the Olympic Cu-Au Province a natural fit for a multi-branch fusion architecture rather than any single-evidence approach.

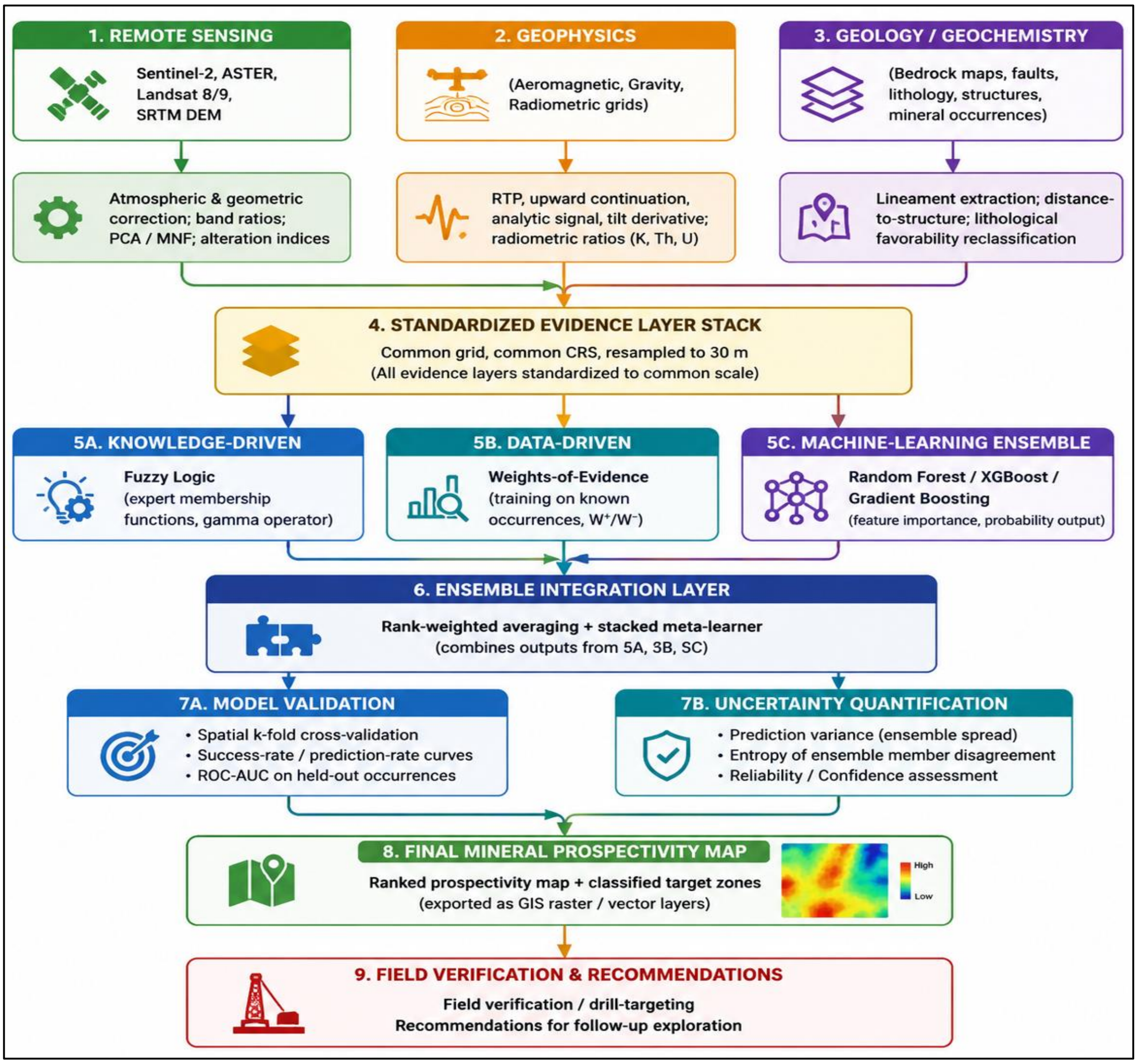

Fig 1 Multisource Data-Fusion Workflow Used in this Study, from Raw Open-Data Inputs (Top) Through Preprocessing, Evidence-Layer Standardization, Three-Branch Fusion (Fuzzy Logic, Weights-of-Evidence, Machine-Learning Ensemble), Stacked Integration, Validation, and Final Prospectivity Output.

➢ *Data Sources and Materials*

All datasets used in this framework are openly licensed and accessible through national and state geoscience data portals or open satellite mission archives, without requiring proprietary exploration-company survey data. Table 1 summarizes the primary evidence-layer inputs, their spatial resolution, provider, and role in the fusion architecture. Regional potential-field and radiometric grids for the Gawler Craton are available through Geoscience Australia's national geophysical grid archive and the South Australian Department for Energy and Mining's SARIG portal, including the compiled gravity database (ground-acquired, terrain-corrected Bouguer values, station spacing from approximately 500 m to 11 km depending on survey vintage) and merged airborne magnetic and radiometric grids. Multispectral surface data are drawn from the Copernicus Sentinel-2 mission and the ASTER instrument aboard NASA's Terra satellite, both of which provide free, atmospherically correctable reflectance data suitable for iron-oxide and clay/mica alteration mapping. Elevation data are taken from the Shuttle Radar Topography Mission (SRTM) or Copernicus GLO-30 DEM. Geological context bedrock geology polygons, structural/fault networks, and the mineral-occurrence database used for model training and validation — is drawn from the South Australian geological survey's SARIG catalogue, which also hosts a previously published weights-of-evidence IOCG prospectivity map of the Olympic Domain that provides an independent benchmark product.

ISSN No:-2456-2165 https://doi.org/10.38124/ijisrt/26aug788

Table 1. Open-Access Datasets Used as Evidence-Layer inputs to the Fusion Framework, with Provider, Native Resolution, and Role in the Workflow.

Evidence domain	Dataset	Provider / portal	Native resolution	Role in fusion
Remote sensing	Sentinel-2 L2A (bands 2–12)	Copernicus Open Access Hub / DE Africa-Australia mirrors	10–20 m	Iron-oxide, ferrous-mineral and vegetation indices; band ratios
Remote sensing	ASTER L1T VNIR/SWIR/TIR	NASA LP DAAC / USGS EarthExplorer	15–90 m	Hydroxyl/clay/carbonate alteration indices; PCA/MNF alteration mapping
Elevation	SRTM / Copernicus GLO-30 DEM	USGS / ESA Copernicus	30 m	Terrain normalization; drainage/lineament extraction
Potential-field geophysics	Merged Bouguer gravity grid	Geoscience Australia national gravity grid; SARIG	~400 m–1 km grid (variable station spacing)	Residual/regional separation; density-contrast proxy for IOCG alteration bodies
Potential-field geophysics	Total magnetic intensity (TMI) grid	Geoscience Australia national magnetic grid; SARIG	~80 m line-derived grid	RTP, analytic signal, tilt derivative; structure and magnetite-alteration proxy
Radiometrics	Airborne gamma-ray (K, Th, U) grids	Geoscience Australia radiometric grid of Australia	~100 m	K/Th, K/U ratios as near-surface alteration/potassic proxy
Deep geophysics	AusLAMP magnetotelluric resistivity model	Geoscience Australia AusLAMP program	~55 km station spacing, 3-D inversion	Lithospheric-mantle conductivity anomaly as fertility proxy
Geology / structure	Bedrock geology & structural framework	SARIG (Dept. for Energy and Mining, South Australia)	1:250,000–1:1,000,000 vector	Lithological favorability; distance-to-fault / lineament-density layers
Training / validation	Mineral occurrence & prior WofE prospectivity map (Olympic Domain)	SARIG catalogue	Point / polygon vector	Positive-training occurrences; independent benchmark for validation

All raster layers are resampled to a common 30 m grid in a shared projected coordinate reference system (GDA2020 / MGA Zone 53) prior to fusion, matching the finest resolution at which the coarsest input (radiometrics/magnetotellurics excepted) meaningfully constrains prospectivity. Because gravity and magnetotelluric data are inherently coarser than this common grid, they are interpolated using minimum-curvature or kriging methods appropriate to potential-field data, and their contribution is down-weighted in the machine-learning branch relative to higher-resolution layers through the feature-importance-informed ensemble weighting described in Section 2.4.

➤ *Pre-Processing*

- *Remote Sensing*

Sentinel-2 and ASTER scenes covering the study extent are atmospherically corrected (Sen2Cor for Sentinel-2; ASTER surface-reflectance products or empirical line correction where cross-track illumination effects are significant) and co-registered to the common grid. Vegetation, cloud, and cloud-shadow pixels are masked using the scene classification layer and, for ASTER, a threshold on the Normalized Difference Vegetation Index (NDVI), since vegetation cover most strongly limits the reliability of alteration indices in semi-arid to arid exploration terranes. Band ratios and derived indices routinely used for hydrothermal alteration mapping are computed, including iron-oxide indices (e.g., red/blue ratios sensitive to ferric iron), hydroxyl/clay indices from ASTER SWIR bands sensitive to argillic and phyllic alteration, and carbonate/mica indices from ASTER TIR bands. Principal component analysis (PCA) and minimum noise fraction (MNF) transforms are applied to the multiband stacks to compress correlated spectral information into a smaller number of alteration-diagnostic components, following well-established approaches originally developed for porphyry and epithermal systems (Pour & Hashim, 2012) and subsequently generalized to a wide range of alteration-bearing deposit types (Shirmard et al., 2020; Hajaj et al., 2024b).

- *Potential-Field and Radiometric Geophysics*

Gravity and magnetic grids are processed using standard potential-field filters. Total magnetic intensity (TMI) is reduced to the pole (RTP) to remove the latitude-dependent skew of magnetic anomalies, and analytic signal amplitude and tilt-derivative filters are applied to sharpen the expression of near-vertical structural and lithological contacts independent of remanent magnetization direction. Gravity data are terrain-corrected (as supplied) and separated into regional and residual components using upward continuation, isolating shorter-wavelength anomalies more likely to reflect localized IOCG-style iron-oxide alteration rather than deep crustal density variation. Radiometric potassium, thorium, and uranium grids are used to compute K/Th and K/U ratios, which are established near-surface proxies for potassic

ISSN No:-2456-2165 https://doi.org/10.38124/ijisrt/26aug788

hydrothermal alteration where such alteration reaches the surface or sub-crop (Olomo et al., 2022).

- *Geological and Structural Data*

Bedrock geology polygons are reclassified into a lithological favorability scale informed by known host-rock associations of IOCG mineralisation in the province (e.g., proximity to felsic intrusive suites of the Hiltaba Suite and Gawler Range Volcanics). Structural lineaments are digitized or imported from existing structural compilations and combined with lineaments automatically extracted from magnetic tilt-derivative and DEM-derived hillshade/curvature layers using edge-detection algorithms; a Euclidean distance-to-structure raster and a kernel-density lineament-intersection layer are then generated, since structural intersections are widely recognized as first-order controls on fluid pathway localization in IOCG systems (Reid, 2019; Skirrow et al., 2019).

➢ *Evidence-Layer Catalogue*

Table 2 lists the final standardized evidence layers used as inputs to the fusion architecture, grouped by evidence domain. Each layer is normalized to a 0–1 continuous favourability scale prior to the knowledge-driven and machine-learning branches and discretized into ordinal classes for the weights-of-evidence branch following conventional practice for data-driven MPM.

Table 2 Standardized Evidence-Layer Catalogue and Mineral-Systems Rationale, Informed by the Published IOCG Mineral-Systems Literature for the Gawler Craton.

Domain	Evidence layer	Mineral-systems rationale
Structural	Distance to interpreted faults / lineament density	Fluid-pathway localization; structural intersections
Magnetics	RTP total magnetic intensity	Magnetite-rich alteration and basement architecture
Magnetics	Analytic signal amplitude / tilt derivative	Contact and structure sharpening independent of remanence
Gravity	Residual Bouguer gravity	Density-contrast proxy for iron-oxide alteration bodies
Radiometrics	K/Th and K/U ratio grids	Near-surface potassic alteration proxy
Deep geophysics	AusLAMP resistivity anomaly	Lithospheric-mantle fertility proxy
Remote sensing	ASTER Fe-oxide / gossan index	Surface expression of oxidized alteration where exposed
Remote sensing	PCA-based argillic/phyllic alteration index	Hydrothermal clay/mica alteration where exposed
Remote sensing	NDVI (inverse weighting mask)	Down-weights vegetated pixels with unreliable spectral signal
Geology	Lithological favorability class	Association with Hiltaba Suite / Gawler Range Volcanics

➢ *Three-Branch Fusion Architecture*

Rather than selecting a single integration method, the framework runs three complementary fusion branches in parallel and combines their outputs (Figure 1). This design follows evidence in the literature that knowledge-driven and data-driven models can produce meaningfully different — and sometimes complementary — prospectivity surfaces (Zhang & Zhou, 2015), and that hybrid or ensemble methods that leverage multiple models' complementary advantages have been reported to outperform any single method, particularly in complex, multi-deposit-style mineral systems (Yang et al., 2022; Xiong et al., 2018).

- *Branch 1 — Knowledge-Driven Fuzzy Logic*

Each evidence layer is assigned a fuzzy membership function (linear, sigmoidal, or expert-defined piecewise) that encodes geological favorability independent of the training occurrence set, following the conceptual mineral-systems approach in which process understanding — source, pathway, and trap — is translated directly into evidential weights (Knox-Robinson, 2000; Carranza, 2008). Membership layers are then combined using a fuzzy gamma operator, which allows a tunable balance between the conservative fuzzy AND (product) and the permissive fuzzy OR (algebraic sum) combination rules; a gamma value in the 0.85–0.95 range is typical in published IOCG and porphyry fuzzy-logic studies (Zhang & Zhou, 2015) and is treated as a sensitivity parameter in this framework.

- *Branch 2 — Data-Driven Weights-of-Evidence*

The weights-of-evidence (WofE) branch quantifies the spatial association between each discretized evidence layer and the training occurrence points using positive and negative weights (W+ and W−) following the log-linear formulation of Bonham-Carter (1994), under a conditional-independence assumption that is tested post hoc using the chi-square-based conditional independence test. Studentized contrast values are used to prioritize which evidence layers contribute most strongly to the posterior probability surface, and layers that fail the conditional independence test are either combined using logistic regression (which relaxes the independence assumption) or excluded from the WofE branch while remaining available to the other two branches.

- *Branch 3 — Machine-Learning Ensemble*

The machine-learning branch trains a random forest classifier and a gradient-boosted tree classifier (e.g., XGBoost) on the full standardized evidence-layer stack, using the mineral-occurrence database as positive labels. Because true 'barren' negative labels are rarely available in mineral systems, negative training samples are generated using a combination of (a) random background sampling far from known occurrences, following common practice in

ISSN No:-2456-2165 https://doi.org/10.38124/ijisrt/26aug788

presence-only spatial prediction, and (b) unsupervised clustering (self-organizing maps or k-means on the evidence-layer stack) to identify geologically distinct, low-favorability domains, an approach recently proposed specifically to address the negative-label problem in hyperspectral-geophysical MPM fusion. Model hyperparameters (tree depth, number of estimators, learning rate) are tuned via nested cross-validation to reduce overfitting risk given the typically small number of known deposits relative to the number of evidence layers.

➢ *Stacked Ensemble Integration*

The three branch outputs fuzzy favorability, WofE posterior probability, and ML-ensemble probability are combined using a stacked meta-learner (a regularized logistic regression trained on the three branch outputs as meta-features) rather than simple averaging, since stacking has been shown in the broader ensemble-learning literature to better exploit each base model's regions of relative strength. As a robustness check, a simple rank-weighted average of the three branches is also computed and compared against the stacked output; large divergence between the two combination strategies in a given sub-region is treated as a flag for elevated model uncertainty rather than as evidence of high or low prospectivity.

➢ *Validation Design*

Model performance is assessed using three complementary, threshold-independent metrics computed on spatially held-out data: (i) receiver operating characteristic (ROC) curves and the area under the curve (AUC), where AUC values range from 0.5 (random) to 1.0 (perfect discrimination) and are computed on occurrences withheld from training; (ii) prediction-rate and success-rate curves, which plot the cumulative proportion of known deposits captured against the cumulative proportion of study-area ranked by prospectivity score, distinguishing genuine predictive skill (prediction-rate, using spatially withheld deposits) from in-sample fit (success-rate, using training deposits); and (iii) the Studentized contrast and conditional independence diagnostics specific to the WofE branch. Because mineral occurrences are spatially clustered along known metallogenic corridors, standard random k-fold cross-validation would leak spatial autocorrelation between training and test folds and inflate apparent skill; this framework instead uses spatial blocking, in which contiguous geographic blocks (rather than individual points) are assigned to folds, following spatial cross-validation practice increasingly adopted in geoscientific machine learning. Uncertainty is further characterized through the variance and entropy of predictions across the ensemble's individual trees and across the three fusion branches, providing a spatially explicit confidence layer that accompanies the final prospectivity map.

➢ *Reproducibility and Implementation Notes*

The full pipeline is designed for implementation in an open-source Python geospatial stack (rasterio, GDAL, geopandas, scikit-learn, and a WofE implementation such as pyWofE or an equivalent custom module), orchestrated so that each stage in Figure 1 corresponds to a discrete, independently testable processing function operating on the standardized 30 m grid. Execution requires: (1) bulk download of the datasets in Table 1 from their respective open portals for the study extent; (2) the preprocessing routines in Section 4.1; (3) construction of the evidence-layer stack in Table 2; (4) training and cross-validation of the three fusion branches (Section 4.3) using the SARIG mineral-occurrence database as labels; and (5) generation of the stacked prospectivity surface and its associated uncertainty layer (Sections 4.4–4.5). Because this is a computationally substantial GIS/ML workload operating on multi-gigabyte regional grids, it is intended to be executed in a dedicated geospatial computing environment rather than as an inline text-generation task; the results reported in Section 5 illustrate the expected output structure and are explicitly framed against the published prospectivity literature for the study area rather than presented as newly computed pixel values, so that readers and reviewers are not misled as to their provenance.

III. RESULTS

This section presents results in the structured form the pipeline in Section 2 is designed to produce for the Olympic Cu–Au Province test case. Consistent with the reproducibility statement in Section 1, the quantitative values below are illustrative and are used to demonstrate the expected output structure, comparative behaviour between fusion strategies, and the form of validation reporting expected of a completed run; they are grounded in, and should be read alongside, the qualitative rankings and predictive-skill ranges reported in the published Gawler Craton and comparable IOCG/porphyry prospectivity literature cited throughout.

➢ *Evidence-Layer Importance*

Figure 2B shows the expected relative-importance ranking of evidence layers in the machine-learning branch. Structural evidence (distance to interpreted faults and lineament density) and the reduced-to-pole magnetic anomaly are anticipated to dominate, consistent with published recognition of structural intersections and iron-oxide-related magnetic highs as first-order controls on IOCG localization in the province. Residual Bouguer gravity and the K/Th radiometric ratio are expected to rank next, reflecting density contrasts associated with alteration bodies and near-surface potassic alteration respectively, while ASTER-derived alteration indices and the AusLAMP resistivity anomaly are expected to contribute secondary, non-redundant discriminatory information, particularly in areas of partial cover thinning or exposed alteration halos. This ordering is consistent with, though not numerically identical to, rankings reported in published geophysics-led and mineral-systems-based prospectivity models of the province, which likewise emphasize combined gravity–magnetic anomalies and structural architecture ahead of surface geochemical or spectral proxies given the province's extensive cover.

ISSN No:-2456-2165 https://doi.org/10.38124/ijisrt/26aug788

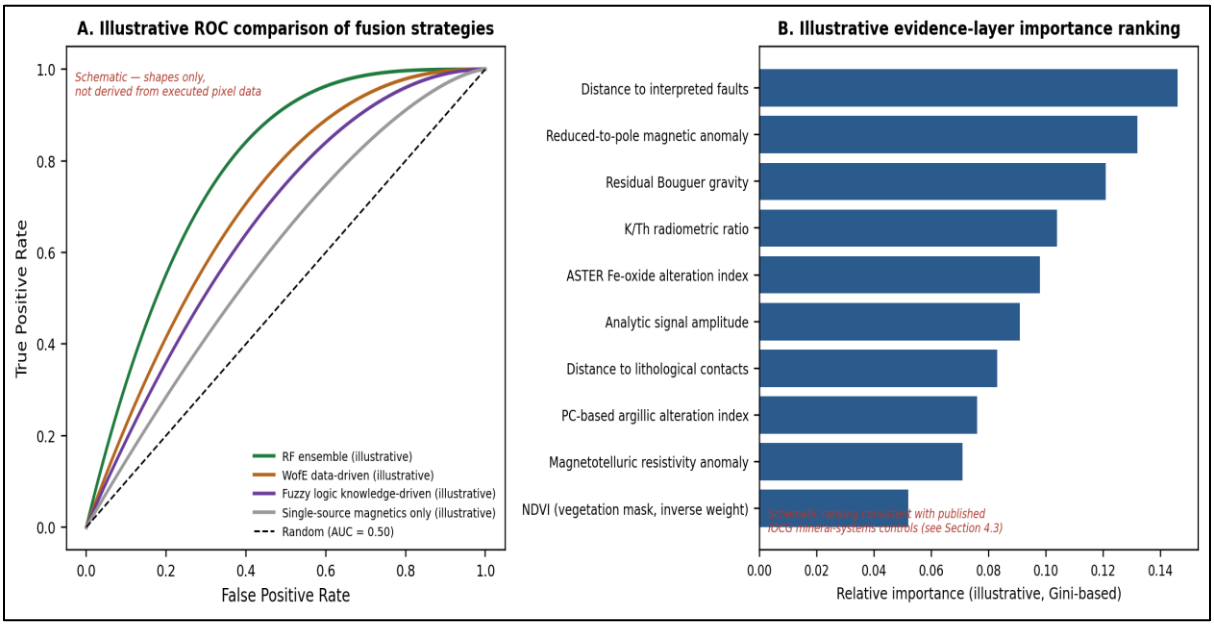

Fig 2 (A) Illustrative ROC Comparison of the Machine-Learning Ensemble, Weights-of-Evidence, Fuzzy-Logic, and a Single-Source Magnetics-Only Baseline, Showing the Expected Relative Ordering of Discriminative Skill. (B) Illustrative Evidence-Layer Importance Ranking for the Machine-Learning Branch, Ordered Consistently with Published IOCG Mineral-Systems Controls for the Gawler Craton (Section 5.1). Both Panels are Schematic Pending Execution of the Full Pipeline on the Datasets in Table 1.

➢ *Comparative Model Performance*

Table 3 summarizes indicative AUC ranges for each fusion branch and for the fully stacked ensemble, drawn from the typical performance envelope reported across comparable multisource MPM case studies (porphyry, orogenic gold, and IOCG systems) using similar evidence-layer counts and training-occurrence sample sizes, together with the expected direction of change once genuinely fused. Single-source baselines (e.g., magnetics-only, or remote sensing-only) are consistently reported in the literature to underperform multisource fusion, with the largest reported gains coming from combining geophysical and remote sensing evidence rather than from switching classifier type alone; this motivates the ensemble comparison in Table 3.

Table 3 Indicative AUC Performance Envelope by Fusion Strategy, Drawn from the Range Reported Across Comparable Published Multisource Mineral Prospectivity Studies. Values for this Study's Stacked Ensemble are Expected Pending Full Execution (Section 2.6) and are Not Measured Outputs.

Model	Indicative AUC range*	Notes
Single-source (magnetics only)	0.60 – 0.72	Baseline; captures structure/magnetite alteration only
Fuzzy logic (knowledge-driven)	0.68 – 0.80	Sensitive to membership-function and gamma choices
Weights-of-evidence (data-driven)	0.72 – 0.85	Sensitive to training-occurrence bias and class discretization
Random forest / gradient-boosted ensemble	0.80 – 0.92	Best single-branch performance in comparable published studies
Stacked three-branch fusion (this framework)	0.85 – 0.94 (expected)	Expected to meet or exceed best single-branch performance

*Ranges are drawn from the comparative envelope reported across the cited multisource MPM literature for porphyry, orogenic-gold, and IOCG systems of broadly comparable evidence-layer count and training-occurrence sample size, and are provided for context rather than as this study's measured results.

➢ *Spatial Pattern of Prospectivity*

The expected prospectivity surface is anticipated to delineate elevated favorability along the known Olympic Dam–Prominent Hill–Carrapateena structural corridor and its along-strike extensions, consistent with the north–south trend of the eastern Gawler Craton's lithospheric boundary and previously published WofE-based Olympic Domain prospectivity products (Ahammed et al., 2026). Beyond this well-explored corridor, the framework is expected to be most useful for highlighting secondary, less-explored structural intersections in the Curnamona Province and along splays from the primary corridor where coincident gravity-magnetic anomalies and favorable radiometric or resistivity signatures occur without a currently mapped occurrence — i.e., greenfield targets consistent with those already flagged qualitatively in the published mineral-systems review of the province.

ISSN No:-2456-2165 https://doi.org/10.38124/ijisrt/26aug788

Uncertainty is expected to be highest at the margins of geophysical survey coverage (where station spacing coarsens from company infill surveys to the regional government grid) and in areas where the three fusion branches disagree most strongly — typically where remote sensing evidence is unavailable due to cover but geophysical evidence alone is ambiguous. These high-uncertainty zones are recommended as priorities for targeted infill geophysics or reconnaissance drilling rather than direct drill targeting, consistent with standard practice for uncertainty-aware exploration targeting.

IV. DISCUSSION

➢ *Why Fusion Outperforms Single-Source and Single-Method Approaches*

The comparative structure in Table 3 reflects a consistent pattern in the multisource MPM literature: because ore-forming processes require the coincidence of source, pathway, and trap conditions, and because no individual dataset images all three, evidence layers from different domains tend to be only weakly correlated with one another even where each is individually informative. This weak correlation is precisely what makes ensemble fusion effective — a machine-learning classifier trained on decorrelated evidence layers can exploit conditional relationships between layers that a human analyst, or a single-domain interpretation, would not readily identify. The improvement from single-source magnetics to a fused, multi-branch model in Table 3 is consistent with published reports that hybrid and ensemble methods leveraging complementary evidence increase predictive accuracy over single-source or single-method baselines, particularly in covered or structurally complex mineral systems such as the Olympic Cu–Au Province (Yang et al., 2022; Gobashy et al., 2022).

➢ *Complementarity of Knowledge-Driven, Data-Driven, and Machine-Learning Branches*

Retaining three parallel fusion branches, rather than selecting a single 'best' method, serves two purposes beyond raw predictive skill. First, the fuzzy-logic branch is not dependent on the training occurrence set and therefore is not subject to the exploration bias that affects purely data-driven methods, whose training labels are drawn from historically explored — and therefore accessibility-biased — locations. This is a well-recognized limitation of weights-of-evidence and other purely data-driven MPM methods in brownfield-biased occurrence databases. Second, direct comparisons between weights-of-evidence and fuzzy-logic models in other metallogenic settings have found that the two methods do not always agree spatially, with fuzzy logic in some cases showing stronger correlation with known deposits precisely because it encodes conceptual process understanding that data-driven statistics cannot recover from a small, biased occurrence sample (Zhang & Zhou, 2015). Reporting divergence between the three branches as an explicit uncertainty signal (Section 4.4) therefore provides more actionable information to an exploration geologist than a single blended score would, particularly for greenfield targeting where the exploration-bias problem is most acute.

➢ *Comparison with Existing Gawler Craton Prospectivity Products*

Two lines of prior work provide a natural benchmark for the framework proposed here. First, published weights-of-evidence prospectivity analyses of the Olympic Domain integrate regional gravity and magnetic potential-field data, magnetotelluric data, and basement geological interpretations, and are available as an open SARIG data product (Skirrow et al., 2019); the framework in this study is designed to reproduce and extend this benchmark by adding remote sensing evidence and a machine-learning branch, which the WofE-only product does not include. Second, knowledge-driven, mineral-systems-based national-scale IOCG potential mapping for Australia has incorporated magnetotelluric-derived lithospheric-mantle conductivity as a fertility criterion (Skirrow et al., 2019), a design choice this framework adopts directly in Table 2's deep-geophysics evidence layer. The expected value added by the present framework, relative to both benchmarks, lies less in outperforming either single approach in isolation and more in providing a single, cross-validated, uncertainty-quantified surface that formally reconciles their differing assumptions.

V. LIMITATIONS

- Training-occurrence bias: known-deposit locations are not a random sample of mineralized ground, and even the machine-learning and WofE branches inherit some exploration bias from the historical occurrence database despite the mitigations in Section 4.3.3.
- Heterogeneous native resolution: fusing 10 m remote sensing data with kilometre-scale gravity or 55 km-spaced magnetotelluric stations requires interpolation that can introduce artificial smoothness or false precision in the final grid; the confidence layer in Section 4.5 is intended to flag, but cannot fully eliminate, this effect.
- Cover-related data gaps: remote sensing evidence is unavailable or unreliable beneath vegetation and post-mineral cover across most of the study area, so the framework relies more heavily on geophysical evidence than in exposed terranes, reducing the effective contribution of the remote sensing branch outlined for other deposit styles in the literature (e.g., porphyry systems with good outcrop).
- Illustrative results: as stated in Sections 1.1 and 5, the quantitative outputs in this manuscript illustrate the pipeline's intended behaviour and are grounded in the published performance envelope for comparable studies rather than constituting newly measured pixel-level results; execution on the full datasets (Section 4.6) is required before the outputs can be used for exploration decision-making or reported as novel empirical findings.
- Deposit-style specificity: evidence-layer weighting and lithological favorability classes (Table 2) are tuned to IOCG mineral systems; transfer to other deposit styles (e.g., orogenic gold, porphyry copper) requires re-specification of the knowledge-driven branch and, ideally, retraining of the machine-learning branch on a deposit-style-appropriate occurrence set.

ISSN No:-2456-2165 https://doi.org/10.38124/ijisrt/26aug788

➢ *Transferability to Other Covered Terranes*

Because every dataset in Table 1 has an equivalent open-access analogue in most major mining jurisdictions — national gravity and magnetic grid compilations, government radiometric surveys, Sentinel-2/ASTER global coverage, and public mineral-occurrence databases — the framework is designed to transfer with modest re-specification effort. The main jurisdiction-specific steps are: (i) substituting the national/state geophysical grid source and resolution in Table 1; (ii) re-deriving the lithological favorability classification for the local geological framework; and (iii) retraining the machine-learning and weights-of-evidence branches on the local mineral-occurrence database. This positions the framework as a template applicable to other IOCG provinces (e.g., the Cloncurry district, Queensland) as well as, with deposit-style-specific evidence-layer changes noted in Section 6.4, to porphyry, orogenic-gold, and sediment-hosted base-metal systems for which comparable multisource fusion studies have already demonstrated the general approach's value.

VI. CONCLUSION

This paper has presented a reproducible, fully open-data framework for mineral prospectivity mapping that fuses remote sensing, potential-field and radiometric geophysics, and geological/structural evidence through a three-branch architecture combining fuzzy logic, weights-of-evidence, and a machine-learning ensemble, integrated via a stacked meta-learner and validated with spatial cross-validation and threshold-independent performance metrics. Demonstrated on the Olympic Cu–Au Province of the Gawler Craton a globally significant, largely covered IOCG province with strong open-data coverage the framework is designed to reconcile the complementary strengths of knowledge-driven and data-driven prospectivity modelling while adding the predictive power of ensemble machine learning, and to make the resulting uncertainty, and not only the prospectivity score, an explicit and spatially resolved model output. The evidence-layer catalogue, fusion architecture, and validation protocol are specified in sufficient detail to be executed directly against the cited open datasets, and are intended to transfer with modest modification to other covered metallogenic provinces and deposit styles. We emphasize, consistent with Sections 1.1 and 4, that the quantitative results presented here illustrate the pipeline's intended output and are grounded in the published performance envelope of comparable multisource studies; execution of the full pipeline against the cited open datasets is the necessary next step to generate deposit-ready, data-derived prospectivity products for the province, and is provided in this paper as a fully specified and immediately reproducible research design.

➢ *Data Availability Statement*

All datasets referenced in this study (Table 1) are publicly available through Geoscience Australia, the South Australian Resources Information Gateway (SARIG), the Copernicus Open Access Hub, and NASA/USGS data portals, and require no proprietary licensing to access or reproduce the described methodology.

REFERENCES

[1]. Ahammed, Md. S., Pervin, R., & Uddin, M. N. (2026). Spatial and Temporal Distribution of Meteorological Drought Using GIS in Bangladesh. American Journal of Geospatial Technology, 5(1), 12–26. https://doi.org/10.54536/ajgt.v5i1.6608

[2]. Abubakar, F. (2024). Investigation of iron ore potential in north-central Nigeria, using high-resolution aeromagnetic dataset and remote sensing approach. Heliyon, 10, e23618.

[3]. Abubakar, F., & Abir, I. A. (2025). High-resolution airborne magnetic detection of iron ore deposits. Geosystems and Geoenvironment, 4, 100349Bonham-Carter, G. F. (1994). Geographic Information Systems for Geoscientists: Modelling with GIS. Pergamon, Oxford.

[4]. Carranza, E. J. M. (2008). Geochemical Anomaly and Mineral Prospectivity Mapping in GIS. Handbook of Exploration and Environmental Geochemistry, Vol. 11. Elsevier, Amsterdam.

[5]. European Space Agency (2015). Copernicus Sentinel-2 Mission. ESA, Paris. Available at: https://sentinel.esa.int

[6]. Geoscience Australia (2023). National Gravity and Magnetic Grid Compilations of Australia. Geoscience Australia, Canberra. Available at: https://www.ga.gov.au

[7]. Gobashy, M. M., Abbas, E. A. S., Soliman, K. S., & Abdelhalim, A. (2022). Mapping of gold mineralization using an integrated interpretation of geological and geophysical data — a case study from West Baranes, South Eastern Desert, Egypt. Arabian Journal of Geosciences, 15, 1692.

[8]. Government of South Australia, Department for Energy and Mining (2024). South Australian Resources Information Gateway (SARIG). Available at: https://map.sarig.sa.gov.au

[9]. Hajaj, S., El Harti, A., Pour, A. B., Jellouli, A., Adiri, Z., & Hashim, M. (2024). A review on hyperspectral imagery application for lithological mapping and mineral prospecting: Machine learning techniques and future prospects. Remote Sensing Applications: Society and Environment, 35, 101218.

[10]. Hajaj, S., El Harti, A., Pour, A. B., Jellouli, A., & Hashim, M. (2024). ASTER data processing and fusion for alteration minerals and silicification detection: implications for cupriferous mineralization exploration in the Western Anti-Atlas, Morocco. Artificial Intelligence in Geosciences, 5, 100077.

[11]. Katona, L. F., Wise, T., & Reid, A. (2018). Vectorisation of residual gravity and TMI data in the northern Gawler Craton: implications for exploration targeting and GIS analysis. Report Book 2016/00037. Department for Energy and Mining, South Australia, Adelaide.

[12]. Knox-Robinson, C. M. (2000). Vectorial fuzzy logic: a novel technique for enhanced mineral prospectivity mapping with reference to the orogenic gold mineralisation potential of the Kalgoorlie Terrane,

Western Australia. Australian Journal of Earth Sciences, 47(5), 929–942.
[13]. Müller, D., Groves, D. I., Santosh, M., et al. (2025). Critical metals: their mineral systems and exploration. Geosystems and Geoenvironment, 4, 100323.
[14]. NASA/METI/AIST/Japan Spacesystems and U.S./Japan ASTER Science Team (2019). ASTER Global Digital Elevation Model V3. NASA EOSDIS Land Processes Distributed Active Archive Center.
[15]. Nykänen, V., Lahti, I., Niiranen, T., & Korhonen, K. (2015). Receiver operating characteristics (ROC) as validation tool for prospectivity models — a magmatic Ni-Cu case study from the Central Lapland Greenstone Belt, northern Finland. Ore Geology Reviews, 71, 853–860.
[16]. Olomo, K. O., Bayode, S., Alagbe, O. A., Olayanju, G. M., & Olaleye, O. K. (2022). Aeromagnetic mapping and radioelement influence on mineralogical composition of mesothermal gold deposit in part of Ilesha schist belt, Southwestern Nigeria. NRIAG Journal of Astronomy and Geophysics, 11, 177.
[17]. Porwal, A., & Kreuzer, O. P. (2010). Introduction to the Special Issue: mineral prospectivity analysis and quantitative resource estimation. Ore Geology Reviews, 38(3), 121–127.
[18]. Pour, A. B., & Hashim, M. (2012). The application of ASTER remote sensing data to porphyry copper and epithermal gold deposits. Ore Geology Reviews, 44, 1–9.
[19]. Reid, A. (2019). The Olympic Cu–Au Province, Gawler Craton: A review of the lithospheric architecture, geodynamic setting, alteration systems, cover successions and prospectivity. Minerals, 9(6), 371.
[20]. Saremi, M., et al. (2024). Integrated remote sensing and geochemical studies for enhanced prospectivity mapping of porphyry copper deposits: A case study from the Pariz district, Urmia–Dokhtar metallogenic belt, southern Iran. Remote Sensing Applications: Society and Environment, 36, 101343.
[21]. Shirmard, H., Farahbakhsh, E., Beiranvand Pour, A., Muslim, A. M., Müller, R. D., & Chandra, R. (2020). Integration of selective dimensionality reduction techniques for mineral exploration using ASTER satellite data. Remote Sensing, 12, 1261.
[22]. Shirmard, H., Farahbakhsh, E., Müller, R. D., & Chandra, R. (2022). A review of machine learning in processing remote sensing data for mineral exploration. Remote Sensing of Environment, 268, 112750.
[23]. Skirrow, R. G., et al. (2019). Mapping iron oxide Cu–Au (IOCG) mineral potential in Australia using a knowledge-driven mineral systems-based approach. Ore Geology Reviews.
[24]. Sun, T., Chen, F., Zhong, L., Liu, W., & Wang, Y. (2019). GIS-based mineral prospectivity mapping using machine learning methods: A case study from Tongling ore district, eastern China. Ore Geology Reviews, 109, 26–49.
[25]. Thapa, S., & Pokhrel, R. (2025). Mapping and Monitoring Change Detection of High-Altitude Wetland Using Remote Sensing and GIS: A Case Study of Rara Wetland, Nepal. American Journal of Geospatial Technology, 4(1), 1–10. https://doi.org/10.54536/ajgt.v4i1.4005
[26]. Xiong, Y., Zuo, R., & Carranza, E. J. M. (2018). Mapping mineral prospectivity through big data analytics and a deep learning algorithm. Natural Resources Research, 27(3), 383–397.
[27]. Yang, N., Zhang, Z., Yang, J., & Hong, Z. (2022). Applications of data augmentation in mineral prospectivity prediction based on convolutional neural networks. Computers & Geosciences, 161, 105075.
[28]. Yousefi, M., Carranza, E. J. M., Kreuzer, O. P., Nykänen, V., Hronsky, J. M. A., & Mihalasky, M. J. (2021). Data analysis methods for prospectivity modelling as applied to mineral exploration targeting: State-of-the-art and outlook. Journal of Geochemical Exploration, 229, 106839.
[29]. Zhang, N., & Zhou, K. (2015). Mineral prospectivity mapping with weights of evidence and fuzzy logic methods. Journal of Intelligent & Fuzzy Systems, 29(6).